Small-angle x-ray diffraction of Kr in mesoporous silica: Effects of microporosity and surface roughness

T. Hofmann, D. Wallacher, P. Huber, R. Birringer, and K. Knorr
Technische Physik, Universität des Saarlandes, D-66041 Saarbrücken, Germany

A. Schreiber and G. H. Findenegg
Stranski-Laboratorium für Physikalische und Theoretische Chemie, TU D-14109 Berlin, Germany
(Received 22 February 2005; published 31 August 2005)

Kr has been adsorbed in SBA-15, a template-grown mesoporous silica substrate. A volumetric adsorption isotherm is presented. The Bragg peaks of the pore array have been measured by small angle x-ray diffraction and analyzed as function of the filling fraction in terms of the electron density contrast, the radial position of the liquid-vapor interface, and film roughness, both for the regime of film growth and capillary condensation. The results are compared with the theory of Saam and Cole. It is shown that the microporosity of the matrix leads to a delay of capillary condensation. The peculiar dependence of the film thickness on the filling fraction points to a high fractal dimension of the pore walls.

DOI: 10.1103/PhysRevB.72.064122 PACS number(s): 81.07.−b, 64.70.Fx, 05.70.Np, 61.10.Eq

I. INTRODUCTION

Capillary condensation, the vapor-liquid transition in confinement, is not only a problem in its own right, but is also of practical importance for the determination of pore size in porous and granular media from adsorption isotherms.[1] The fundamental aspects of this transition are known for a long time, we refer in particular to the theory of Saam and Cole[2] (SC), which not only covers capillary condensation but also the preceding growth of the adsorbate on the pore walls. More recently the interest has shifted to capillary condensation in disordered pore networks, as, e.g., realized in porous Vycor glass or aerogels. Here collective effects lead to the prevalence of metastable states.[1,3]

The advent of template-based preparation techniques has supplied us with substrates that have very regular pores. The pores of SBA-15 are linear, nonramified, they are all parallel and form a two-dimensional (2-D) hexagonal array, as has been shown by electron microscopy and small angle diffraction.[4] This material is expected to come close to an ensemble of independent homogeneous cylindrical pores of uniform cross section. We will study capillary condensation and film adsorption by combining the measurement of a volumetric adsorption isotherm with small angle x-ray diffraction on the pore array. Kr has been chosen as adsorbent, not only because it is a simple rare gas atom, but also because the Kr electron density is close to that of the silica matrix. Thus the diffracted intensity mainly stems from the contrast between the empty (=vapor filled) regions and the Kr/silica composite. This will simplify the analysis of the x-ray data. The present work was also stimulated by small angle neutron diffraction results[5,6] on N_2 in SBA-15.

II. EXPERIMENTAL

SBA-15 silica was synthesized according to the prescription of Zhao *et al.*[7,8] using the triblock copolymer $PEO_{17}-PPO_{54}-PEO_{17}$ (Pluronic P103 from BASF) as the structure-directing template and tetraethyl orthosilicate (TEOS) as the silica source. A solution 4 g P103 and 23.9 g H_2SO_4 (97%) in 240 g pure water was mixed with 8.6 g TEOS at 35 °C and kept at this temperature under constant stirring for 5 h. The heterogeneous reaction mixture was then submitted to hydrothermal treatment at 105 °C in the reaction vessel for 24 h. The as-synthesized material obtained by filtration and washing with pure water was dried, first at 105 °C and then at 180 °C, for several hours, and finally calcined at 550 °C in air.[9]

A metallic cell equipped with two planar parallel Be windows was stuffed with the SBA-15 powder. The gap between the windows was 0.3 mm. The sample was outgassed at 120 °C at a pressure below 10^{-5} mbar. The cell was mounted to a closed cycle He refrigerator and was cooled down to 119 K. The temperature stability was better than 2 mK. High purity Kr gas was admitted into the cell, respectively, removed from the cell in small, volumetrically controlled portions via a heated fill line. The Kr vapor pressure was measured with a membrane-type gauge with capacitive read-out (Baratron, 1000 mbar full scale). For each such adsorption or desorption step, the change of pressure with time was monitored and the new asymptotic pressure value was obtained by fitting a stretched exponential decay law to the data.[10] The resulting adsorption/desorption isotherm in reduced form, f, as a function of p, is shown in Fig. 1. The fractional filling f is the mass uptake normalized to the complete filling and p is the relative vapor pressure. (The saturated vapor pressure at 119 K is 955 mbar). For most data points the small angle x-ray diffraction pattern was recorded. MoK_α radiation emanated from a rotating anode was reflected from a graphite (002) monochromator, passed through the sample, and exposed an image plate. The total length of the x-ray path was 4 m, the exposure time 4 h. The image has perfect rotational symmetry, the sample is a powder, not only in the morphologic but also in the crystallographic sense. The distance from the center gives the momentum transfer modulus q. As can be seen from Fig. 2, the

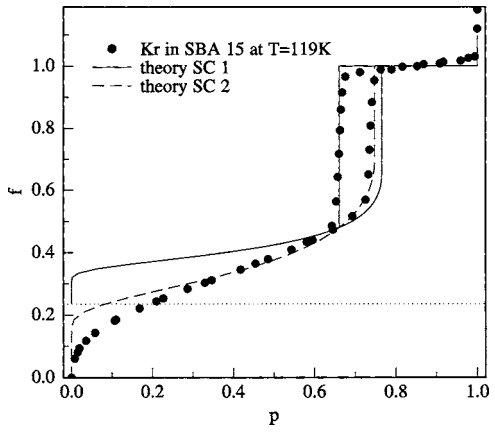

FIG. 1. Volumetric adsorption isotherm of Kr in SBA-15 at 119 K. f is the fractional filling, p the relative vapor pressure. The solid lines are two fits of the SC model to the data.

radial distribution of the scattered intensity $I(q)$ shows five peaks. The width of these peaks was studied for various cross sections of the x-ray beam. The intensity I_0 of the direct beam after the sample was monitored. I_0 decreases exponentially with increasing Kr uptake f of the porous matrix, $I_0(f)=I_0(f=0)\exp(-\mu f)$, $\mu=1.52$.

III. DATA ANALYSIS

Gaussian profiles sitting on a smooth background have been fitted to the peaks of the diffraction patterns. The peak positions are consistent with a 2D triangular lattice with the lattice parameters $a=b=(10.80\pm0.05)$ nm, $\gamma=120°$. The peaks are indexed (10), (11), (20), (21), (30). All peaks have the same intrinsic width that translates into a coherence length of the 2D lattice of 200 nm. This is about the size of the powder grains. Referring to the transmission data, the integrated peak intensities have been corrected for the f-dependent absorption. This means that there is a common scale factor C for the complete set of Bragg intensities obtained at different values of q and f.

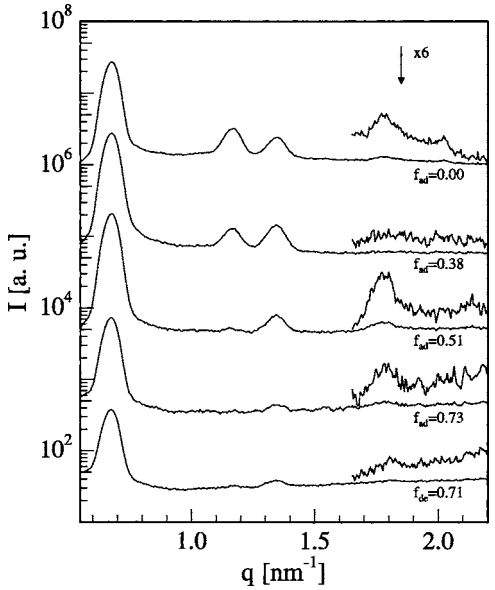

FIG. 2. The intensity profile of the small angle scattering experiment. q is the modulus of the scattering vector. The selected filling fractions f are indicated. The top four curves refer to the adsorption, and the bottom curve to the desorption branch of the isotherm. The curves are shifted vertically by one decade with respect to each other.

The size of the lattice parameter combined with a rough estimate of the pore diameter as derived from the characteristics of the template, the reduced vapor pressure of the capillary condensate, and electron microscopy images suggest that the 2D unit mesh hosts just one pore. We assume that the pores are cylinders, aligned along the z direction, perpendicular to the 2D lattice. The extension of the pores in the z direction is large compared to the lattice parameter. Otherwise, the Bragg peaks would have an asymmetric shape with a longer tail on the high-q side, thereby approaching the Warren lineshape[11] in the limit of zero extension along z.

For the values of q probed in a small angle scattering experiment, the atomistic structure of the sample is irrelevant; the wall material and the Kr pore filling can be represented by average electron densities ρ. The problem is to find a radial electron density profile $\rho(r)$ that fits the Bragg intensities, as measured at different filling levels with a minimum number of adjustable parameters.

The adsorption/desorption isotherm consists of an initial part that is reversible on adsorption and desorption. Here an adsorbed liquid film grows on the pore walls, the thickness t of which increases with increasing p. Eventually at a critical thickness t_c^{ads} (or equivalently at a critical filling fraction f_c^{ads} and at a critical value r_{Ic}^{ads} of the radius r_I of the empty core in the pore center), the cylindrical vapor-film interface turns instable and biconcave parcels of capillary condensate form. Complete filling is then achieved by the further condensation of vapor onto the menisci such that they advance along the pores toward the pore mouths. On desorption the capillary condensate evaporates, the menisci retreat, and the capillary condensate finally disappears at f_c^{des}. At this moment the thickness of the adsorbed film on the pore walls is $t_c^{\mathrm{des}}, t_c^{\mathrm{des}} < t_c^{\mathrm{ads}}$. The SC theory[2] describes these events, including the hysteresis of capillary condensation on adsorption and desorption.

The combination of this scenario with the approximate electron density matching of liquid Kr and silica suggests a radial profile $\rho(r)$ of the form $\rho=\rho_2$ for $r>r_I$ with $\rho_2\approx\rho_{\mathrm{Kr}}\approx\rho_{\mathrm{SiO_2}}$ and $\rho=\rho_1$ for $r<r_I$ with $\rho_1=0$ in the regime of film growth ($f<f_c$) and with $0<\rho_1<\rho_2$ in the regime of capillary condensation ($f>f_c$). Apart from the common scale factor C, there are two parameters, r_I, and the contrast, $\Delta\rho=\rho_2-\rho_1$, that have to be adjusted for each value of f.

For film growth on smooth walls, the geometric relation $f=1-(r_I/R)^2$ should hold. R is the radius of the empty pores ($f=0$). In the regime of capillary condensation, r_I should be independent of f. In the case of perfect density matching, the Bragg peaks should disappear for complete filling. This situation is, in fact, approached in the experiment. The intensity ratio of the Bragg peaks at $f=1$ and $f=0$ is of the order of 7% when correcting properly for absorption.

It is necessary to include an additional parameter that accounts for the decrease of the Bragg intensities with increasing q. In a first model (model A) this effect is considered by introducing a Debye-Waller-type parameter u, the rms displacement of the pore centers from the regular lattice positions. The integrated intensities (corrected for absorption) of the (hk) powder lines (=Debye-Scherrer rings) are then given by[4]

$$A_{hk} = \Delta\rho r_I \frac{J_1(r_1 q)}{q}, \tag{1}$$

$$I_{hk} = CM_{hk} \frac{A_{hk}^2}{q} \exp(-q^2 u^2/2). \tag{2}$$

J_1 is the first-order Bessel function, M_{hk} is the peak multiplicity (=12 for the (21) peak, =6 for the others).

In the alternative model B, the "corona" model of Ref. 4, u, is set to zero and the density step at r_I is replaced by a linear ramp extending from ρ_1 at $r_I - \delta$ to ρ_2 at $r_I + \delta$. This has a similar effect on the q dependence of the Bragg peaks. Both models fit the data well. The f dependence of the parameters is shown in Fig. 3. Table I compares the experimental and calculated peak intensities for some selected values of f. The quality of the fit is also documented in Fig. 4, which compares the radial electron density profile as obtained from a fit of model B to the $f=0.31$ data, with the result of a Fourier transformation of the Bragg amplitudes $\pm I_{hk}^{0.5}$ into real space. In a centrosymmetric structure, the phase problem of crystallography is reduced to unknown signs of the Bragg amplitudes. The signs have been taken from the fit of the models to the data. For $f=0.31$, the nodes of the pore form factor are well separated from the q positions of the Bragg peaks. Hence the choice of the signs is robust.

The reliability of the fit is also documented by the following consistency check, which shows that the filling fraction f_x, as derived from the fit parameters $\Delta\rho$, δ, and r_I of the diffraction experiment, is proportional to the volumetric filling fraction f. For $f < f_c, \Delta\rho$ is equal to ρ_2 and f_x is directly obtained from the change of the integral of $\rho(r)$ over the unit mesh of the pore array with respect to the empty state $(f=0)$. For $f > f_c$, we made the plausible assumption that the further changes of $\Delta\rho$ as a function of f are entirely due to an increase of ρ_1 caused by the spreading of the capillary condensate along the pores.

The low-f limit of r_I is considered the best measure of the nominal pore radius $R, R=(4.15\pm0.05)$ nm. In the regime of capillary condensation r_I is approximately constant, but is different for adsorption and desorption, $r_{Ic}^{\mathrm{ads}}=3.2$ nm and $r_{Ic}^{\mathrm{des}}=3.5$ nm. The limiting thickness $t, t=R-r_I$, of the adsorbed film in coexistence with the capillary condensate is slighty larger on adsorption, but only by less than one monolayer, than on desorption. The porosity of a SBA-15 grain as calculated from R and the lattice parameter a is 0.55. The wall thickness along a line from one pore center to the next is $a-2R=2.4$ nm. The values of R, u, and δ are close to those of sample P123 BC of Ref. 4 that has, in fact, been prepared in a very similar way.

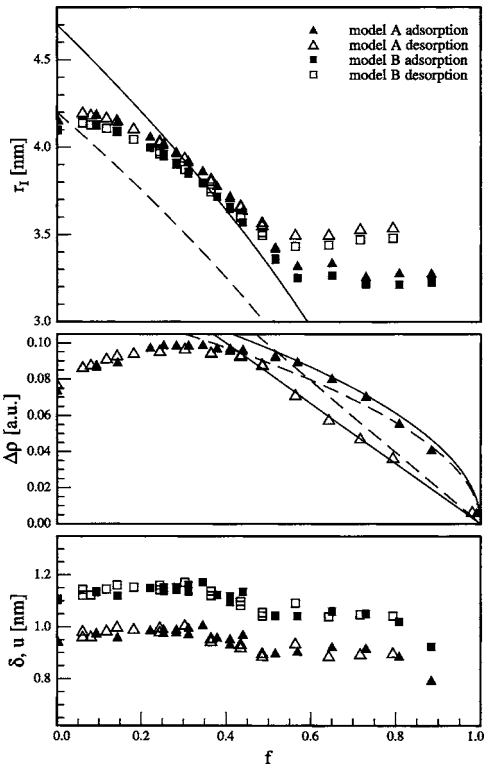

FIG. 3. The fit parameters of models A and B as a function of the filling fraction f. r_I is the (average) radial position of the step of the density contrast $\Delta\rho$ between the pore center and the pore walls, including the adsorbed film; δ and u are measures of the smearing of the step. The symbols indicate whether the data refers to adsorption or desorption, or to model A or B. For the contrast $\Delta\rho$, the results of the two models are indistinguishable. The lines of the top frame are two examples for the geometric relation that describes the growth of an adsorbed film on a smooth wall. The solid and dashed lines of the center frame are the linear and square-root-type dependence expected for the coherent and incoherent summation of Bragg amplitudes.

Figure 5 shows the radial density profile $\rho_{\mathrm{Kr}}(r)$ of Kr for some values of f. It has been obtained from the profile as given by the fit parameters $\Delta\rho, r_I, \delta$ of model B, subtracting the $f=0$ profile. The results shown in this figure demonstrate how the Kr filling spreads out in pore space. The kinks of the profiles result from the subtraction, but should not be overinterpreted. The most surprising aspect is perhaps that for the first adsorption steps the Kr molecules enter into the silica matrix, thereby increasing its electron density rather than forming adsorbate film on the pore walls. This behavior is also apparent from the fact that r_I is about constant at low f (Fig. 3), in clear contradiction to the geometric $r_I - f$ relation expected for film growth on smooth walls. Of course, we wondered whether these results are artifacts arising from an oversimplified model of the radial density profile. Therefore we repeated the fits with $\rho(r)$ profiles that distinguish between the Kr density ρ_{Kr} and the matrix density $\rho_{\mathrm{SiO_2}}$. In order to keep the number of fit parameters in balance with the number of Bragg intensities, we had to impose constraints such as that these two densities as well as the pore radius R are independent of f. Fits of this type turned out to

TABLE I. The integrated Bragg intensities (including absorption) of the diffraction experiment. The numbers in brackets are the values calculated from a fit of model A to the data. "ad" and "de" refer to data obtained on adsorption and desorption, respectively.

	Peak				
f	(10)	(11)	(20)	(21)	(30)
0.00	9185 (9177)	763 (763)	479 (478)	50 (33)	24 (38)
0.10	9719 (9712)	827 (827)	484 (483)	45 (38)	17 (36)
0.16	9222 (9215)	703 (702)	442 (441)	29 (25)	21 (31)
0.31	7380 (7378)	304 (304)	301 (301)	0 (0)	11 (14)
0.35	6894 (6892)	223 (223)	258 (258)	0 (1)	6 (9)
0.49	4659 (4656)	27 (27)	107 (108)	31 (30)	0 (0)
0.79 ad	1055 (1054)	0 (0)	11 (11)	12 (12)	0 (0)
0.72 de	474 (474)	4 (4)	12 (12)	3 (3)	0 (0)

be inferior compared to those presented above. In particular, there is no way to reconcile the dependence of r_I on f with the geometric relation.

The adsorption isotherm is compared with the predictions of the SC theory. This phenomenological theory deals with the liquid-vapor transition in a cylindrical pore with smooth walls. It is based on a nonretarded van der Waals interaction between the matrix and the molecules in the pore. The intermolecular interaction enters via the liquid-vapor surface tension. The reduced isotherms (f vs p) of this model depend on two parameters (the quantities R_0/R and R_T/R of Ref. 2). Two examples of SC isotherms are included in Fig. 1. Here the parameters of the model have been adjusted to reproduce the lower closing point of the hysteresis loop. This implies that p_c^{des} is the equilibrium vapor pressure of the capillary condensate. This is likely to be so, since on desorption there is no need of nucleating vapor bubbles, the pore can empty via the retreat of menisci that already exist at the pore mouth. Variations of the pore diameter along the pore may lead to metastable states on desorption, due to the pore blocking mechanism. See, however, Ref. 10 for the absence of pore blocking in ink-bottle pores. In order to fix the second free parameter of the model, we refer alternatively to the value r_{Ic}^{des} of the scattering experiment (curve SC1) or to the value of f_c^{des} of the experimental isotherm (curve SC2).

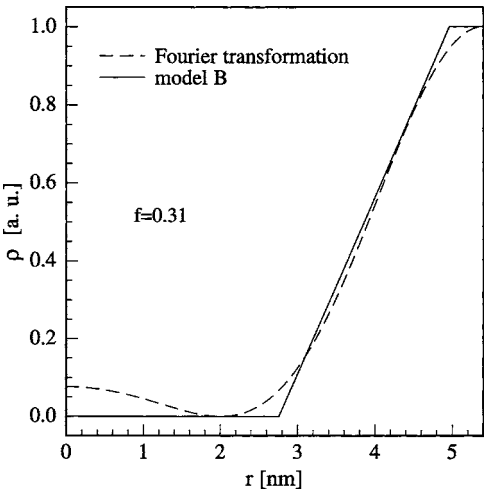

FIG. 4. The radial density profile of $\Delta\rho(r)$ for $f=0.31$ as obtained from the fit of model B compared with the transformation of the Bragg amplitudes into real space.

IV. DISCUSSION

The topics of interest are the thermodynamics of adsorption and capillary condensation and the partition of the pore space in empty and filled regions. Referring to the regime of capillary condensation first, one notes that hysteresis is not only observed in the adsorption/desorption isotherms but also in the f dependence of the structural parameters $\Delta\rho$ and r_I (Fig. 3). r_I is about constant in this regime; the contrast $\Delta\rho$ decreases with increasing f, the pore obvious fill and empty, while the adsorbed film on the pore walls is kept at a constant thickness. For a given value of $f, \Delta\rho$ is lower and r_I is larger for desorption than for adsorption. On desorption there is more capillary condensate and less film condensate. This is consistent with the theoretical model. The SC model overestimates, however, the width $(p_c^{\mathrm{ads}}-p_c^{\mathrm{des}})$ of the hysteresis (Fig. 1). Irregularities of the pore space and fluctuations are expected to induce the nucleation of the capillary condensate before the system has reached the theoretical end point of supersaturation.

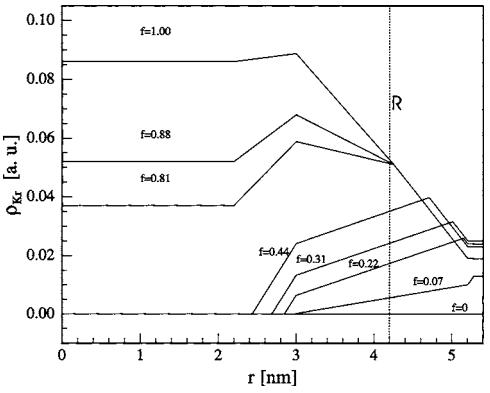

FIG. 5. The radial profile of the Kr density $\rho_{\mathrm{Kr}}(r)$ for some filling fractions f.

There is a marked difference of the f dependence of $\Delta\rho$ between adsorption and desorption. On desorption, $\Delta\rho$ varies approximately linearly with f, whereas the adsorption data follows a nonlinear, almost square-root-like dependence. The linear dependence refers to the "coherent" case, $\rho_1=\rho_2(f-f_c)/(1-f_c)$, where the density ρ_1 of the pore center region takes the same value in every coherence volume (=SBA-15 grain). The "incoherent" square-root behavior describes the other limiting case, where the macroscopic filling fraction f is realized by a coexistence of grains with different filling levels, including the extreme case that some grains are completely filled and others have just an adsorbed film of maximum thickness on the pore walls. The simplest explanation of the coherent behavior observed on desorption refers to independent pores, all having the same size, that empty via a retreat of the menisci at the equilibrium vapor pressure of the capillary condensate. The filling process, on the other hand, is a collective process extending over the whole grain. If once a liquid parcel has nucleated somewhere in the grain, the menisci not only propagate along this pore, but also manage to find their way into neighboring pores, most likely via pore, junctions or cross-links that are due to growth defects of the template lattice that has been used to prepare the porous matrix. For disordered pore networks as, e.g., of Vycor glass, it is usually argued that the situation is reversed. Pore emptying is a collective percolation-type process that involves metastable states, but that on adsorption a pore segment of radius R fills independently of other segments at a pressure that is close to the equilibrium value.[1] For bundles of carbon nanotubes, it has been proposed that the collective nature of the filling process can be due to the fact that the substrate potential in one pore depends on whether neighboring pores are filled or empty.[12,13] We doubt that this view applies given the rather thick interpore walls of the present matrix.

For a film growing on a smooth wall and density matched to the wall material, one expects that $\Delta\rho$ is constant (and equal to ρ_2), and that the radial position r_I changes with f according to the geometric relation $f=1-(r_I/R)^2$. As has been mentioned already above, the experiment is by no means consistent with this relation. At low f, r_I rather approaches a constant value and it is the contrast $\Delta\rho$ that changes with f. The adsorption of Kr does not lead to a film on the pore walls of increasing thickness $t, t=R-r_I$, but the Kr molecules rather penetrate into the matrix material, thereby increasing its electron density ρ_2. The matrix obviously has a spongelike morphology with a lot of pores. For ease of discussion we refer to them as "micropores," without implying that all of them are smaller than the mesopores that form the hexagonal pore array. It has been argued that the microporosity of the pore walls is a consequence of the preparation technique.[4]

One can estimate the porosity P_W of the walls in two alternative ways that, in fact, give similar results but that are both based on the questionable assumption that the filling of the micropores is completed at some low value of $f, f<f_c$. The first model postulates that the walls, which is the medium at distances r from the pore centers with $r>R$, consist of compact SiO_2 and voids. At $f=0.2$, $\Delta\rho$ is maximum, and we assume that this is due to a complete filling of these voids with liquid Kr. The change of $\Delta\rho$ from $f=0$ to $f=0.2$ translates into a porosity P_W of about 0.3. The second approach refers to the comparison of the experimental and the geometric r_I vs f relation. The relation is modified by replacing R by an effective pore radius R_{eff} that is meant to include the void space within the walls. From the experimental value of r_I at $f=0.2$, one obtains $R_{\mathrm{eff}}=4.70$ nm, which again translates into a porosity P_W of about 0.3. Note, however, that neither the original nor the modified geometric r_I-f relation fits the experimental data in an acceptable way. Considering meso as well as micropores, the total porosity of a SBA-15 grain is 0.70. About 20% of a complete filling resides in the micropores.

The theoretical isotherms (SC1 and SC2) of Fig. 1 are chosen in order to agree with the experimental result on the lower closing point of the hysteresis loop. As mentioned already previously, the model overestimates the range of metastability on adsorption. More importantly, the model fails to fit the regime of film growth in an acceptable way. Isotherm SC1 largely underestimates the f width of the film growth regime, the theoretical isotherm starts at about $f=0.2$ on the experimental f scale. This agrees with the conclusions of the last paragraph. The theoretical isotherm SC2 provides, at first glance, a somewhat better fit of the initial reversible part of the isotherm, but a closer look reveals that the monolayer capacity is overestimated. Therefore the values of R and of the critical film thickness t_c derived from SC2 deviate from the results of the diffraction experiment. The geometric relation between f and r_I (or t) is part of the model, the model has to fail in case the walls are not smooth but contain voids.

Nevertheless the experimental isotherm of Fig. 1 is close to ideal in the sense that the adsorption branch is almost vertical, much steeper compared to what we and others have observed for porous glasses, porous Si, and MCM-41 samples. In fact, we only know of one isotherm that looks more ideal, the O_2 isotherm of Awschalom *et al.*[14] on an early example of a template-grown substrate. We have calculated an SC isotherm from the parameters given in this article. The p width of the calculated hysteresis loop is narrower than observed experimentally, in contrast to the present case. The fit to the regime of film growth is poor, quite similar to the quality obtained with curve SC2 in our study. We therefore think that the conclusions of these authors concerning the radii $R, r_{Ic}^{\mathrm{ads}}, r_{Ic}^{\mathrm{des}}$ are incorrect.

The walls are obviously not smooth but rough. It is the corona model B with the parameter δ that considers the roughness in a natural way, $\delta/R\approx 0.25$, even though the diffraction experiment cannot discriminate between the roughness δ of model B and the displacement u of the pores from the lattice sites of model A. The u values obtained are well below the thickness of the interpore walls. This means that the pores rarely touch or overlap. The smearing of the density step could also come from a pore size distribution with a finite variance $\Delta R/R$. Note, however, that the rather steep slope of the branches of the hysteresis loop suggests values of $\Delta R/R$ of 0.025, only.

δ and u change little as a function of f, nevertheless there is a slight drop at the onset of capillary condensation at $f_c\approx 0.5$. At the onset, the adsorbate-vapor interface has advanced to an average distance r_{Ic} from the pore center that

coincides with $R-\delta$. Obviously capillary condensation starts right at the moment when the filling of the micropores in the walls is completed. This is an interesting point. According to the SC theory, capillary condensation is induced by undulation-type fluctuations of the cylindrical liquid-vapor interface. The critical mode is that with an infinite wavelength since it has the largest amplitude. The roughness of walls suppresses long-wavelength modes with the result that capillary condensation is delayed. It is only after the micropores are filled that long-wavelength fluctuations can develop. This explains qualitatively why the f width of the film growth regime is larger than expected theoretically for adsorption on smooth walls.

V. FRACTAL APPROACH

Rough surfaces are characterized by the Hausdorff dimension[15] $D, D>2$. Theories have been developed that treat adsorption on fractal surfaces. It has, e.g., been suggested[16] that the exponent of the FHH isotherm of the multilayer regime gives access to D. Unfortunately such models cannot be applied directly to the present system since the capillary condensation in the mesopores interferes with the multilayer growth on the pore walls. The initial part of the present isotherm, up to about $f=0.4$, can be nicely fitted with a BET isotherm. The fit supplies a monolayer capacity of $f=0.21$. The theoretical curve SC2 (Fig. 1) suggests a similar value. The experimental value is about 0.12, and the value estimated from the size of the Kr molecule in relation to the substrate surface of $2\pi R$ (per unit pore length) is 0.17. The different values can be reconciled by introducing the fractal dimension D of the surface of the order of 3.

The diffraction experiment supplies direct information on the dependence of the adsorbing area $2\pi r_I$ (per unit pore length) as a function of f. This information is, of course, model dependent, but the structural model appears to be reliable and consistent. f is the fraction of pore space occupied by Kr molecules. Hence the r_I-f data establishes a relation between a surface and a volume, which should follow the geometric relation from above generalized to D dimensions, $f=1-(r_I/R)^D$, $D=\log(1-f)/\log(r_I/R)$. At very low f, there is little if any change of r_I, and accordingly D is very large. It is only in a very high-dimensional space that the adsorbed volume can increase without a noticeable increase of film thickness. Even at higher f values within the regime of film growth, $0.3<f<0.5$, the change of r_I (and equivalently t) with f is not consistent with $D=2$, but with D values between 4 and 5. The fractal concept may not be very informative, but it nevertheless demonstrates that the film growth on the pore walls of the present SBA-15 sample is incompatible with $D=2$ for any f.

VI. CONCLUSIONS

Adsorption isotherms are a standard tool for the determination of the average pore diameter and even distributions of the diameter. The pore radius is calculated from p_c^{ads} or p_c^{des} in terms of the Kelvin equation or from the "t approach" that corrects for the finite thickness of the adsorbed film in coexistence with the capillary condensate. Fits of the SC model are perhaps the most sophisticated approach (apart from density functional calculations and computer simulations), but the problem of metastable states remains, in particular, in disordered pore networks, and it is by no means obvious whether for a given porous substrate p_c^{ads} or p_c^{des} is closer to the equilibrium vapor pressure of the capillary condensate. For the present sample such network effects appear to be negligible, but complications arise from the microporosity of the matrix material. Fitting the SC model directly to the isotherm gives a pore diameter that strongly deviates from the diffraction result. Thus, even for a sample that is considered close to perfect, the extraction of geometric information from adsorption isotherms is questionable.

Apart from these practical aspects, the present study has given a detailed insight into the radial distribution of the condensate in the mesopores. The model of Saam and Cole obviously grasps the essentials of adsorption and capillary condensation. Some results are unexpected, namely, the r_I-f relation of film growth, the delay of capillary condensation, which presumably results from the roughness of the pore walls, and the "coherent" versus "incoherent" behavior of the Bragg intensities of the capillary condensation regime. For a more detailed understanding of these effects, the diffuse scattering had to be analyzed, which in turn, would require stronger x-ray sources than just laboratory equipment or light scattering experiments on a single grain. Such experiments could give information on the spatial correlation of the roughness of the pore walls and of the adsorbed film, as well as on the correlations of the menisci of the capillary condensate.

ACKNOWLEDGMENTS

This work has been supported by the Sonderforschungsbereich 277, Saarbrücken, and by the Sonderforschungsbereich 448, Berlin/Potsdam.

[1] Y. C. Yortsos, *Methods in the Physics of Porous Media* (Academic, New York, 1999).

[2] W. F. Saam and M. W. Cole, Phys. Rev. B **11**, 1086 (1975).

[3] E. Kierlik, P. A. Monson, M. L. Rosinberg, L. Sarkisov, and G. Tarjus, Phys. Rev. Lett. **87**, 055701 (2001).

[4] M. Imperor-Clerc, P. Davidson, and A. Davidson, J. Am. Chem. Soc. **122**, 11925 (2000).

[5] A. Schreiber, Ph.D. thesis, Technische Universität Berlin, 2002.

[6] A. Schreiber, I. Ketelsen, G. H. Findenegg, and E. Hoinkis (to be published).

[7] D. Zhao, Q. Huo, J. Feng, B. F. Chmelka, and G. Stucky, J. Am. Chem. Soc. **120**, 6024 (1998).

[8] D. Zhao, J. Feng, Q. Huo, N. Melosh, G. H. Fredrickson, B. F. Chmelka, and G. D. Stucky, Science **279**, 548 (1998).
[9] A. Schreiber, I. Ketelsen, and G. H. Findenegg, Phys. Chem. Chem. Phys. **3**, 1185 (2001).
[10] D. Wallacher, N. Kuenzer, D. Kovalev, N. Korr, and K. Knorr, Phys. Rev. Lett. **92**, 195704 (2004).
[11] L. V. Azaroff, *Elements of X-Ray Crystallography* (McGraw-Hill, New York, 1968).
[12] R. Radhakrishnan, K. E. Gubbins, and M. Sliwinska-Bartkowiak, J. Chem. Phys. **111**, 1147 (2002).
[13] M. W. Cole, V. H. Crespi, G. Stan, C. Ebner, J. M. Hartmann, S. Moroni, and M. Boninsegni, Phys. Rev. Lett. **84**, 3883 (2000).
[14] D. D. Awschalom, J. Warnock, and M. W. Shafer, Phys. Rev. Lett. **57**, 1607 (1986).
[15] B. B. Mandelbrot, *The Fractal Geometry of Nature* (W. H. Freeman, San Fransisco, 1982).
[16] P. Pfeifer, Y. J. Wu, M. W. Cole, and J. Krim, Phys. Rev. Lett. **62**, 1997 (1989).